Investigation of Mixing in a Turbofan Exhaust Duct, Part II: Computer Code Application and Verification

Louis A. Povinelli* and Bernhard H. Anderson†
NASA Lewis Research Center, Cleveland, Ohio

The analysis and computational procedure in Part I of this paper was used to compute several three-dimensional lobe mixer flow fields in various geometries for which experimental data were available. Detailed measurements, including flow angularity data at the inlet to the mixing duct, were obtained and a model of the initial secondary flow was developed for use with the computational procedure. It is shown that for both warm and hot flow configurations excellent agreement between the predicted and measured total temperature signatures at the mixing duct exit plane can be obtained when the secondary flows on the initial plane are accounted for in the initial conditions. From this series of calculations and comparison with data, it is concluded that secondary flow convective effects generated within the lobes, rather than turbulent transport effects, play the dominant role in determining the characteristics of the mixing process downstream of the lobe exit plane. These results provide additional insight of the mixing process and demonstrate that the analysis developed in Part I of this paper can satisfactorily predict the flow development within lobe mixer exhaust ducts.

Introduction

SIGNIFICANT performance gains can be achieved in turbofan engines by mixing the hot core stream with the cooler fan stream prior to expansion through the exhaust nozzle. Theoretical thrust gains for ideal mixing and scale mode test results have been published by Frost[1] and Hartmann.[2] The amount of performance gain depends on the balance between the degree of mixing of the hot and cold streams, and the pressure losses incurred during the mixing process. Over the last several years, a variety of mixer configurations have been tested; for example, in Ref. 3 confluent, injection, vortex generator, and multilobe chute geometries have been investigated. Of all the geometries tested to date, the lobe mixer has been the most successful for promoting mixing and minimizing losses. The design of the lobe mixers has been based on quasiempirical methods and intuition, and the performance determined through experimentation.[3-5] These experiments were sufficient to determine the relative merits of one lobe geometry over another. However, in the absence of a complete understanding of the mixing process, conclusions reached with one series of tests could not be extrapolated to the next generation of mixer nozzles. This reinforces the need for analytical procedures capable of predicting flows within lobe mixer geometries. Aerodynamic analysis for the design of mixer nozzles was first published by Birch et al.[6] Predictions were made for the total temperatures and velocities at the nozzle exit plane for both full-scale and model mixers. Since detailed knowledge of the flowfield at the exit of the mixers was not available, a set of inlet conditions was selected consistent with the known integral values of the flow. Comparison of the computed and experimental results showed encouraging results. The need for defining local flow properties, especially at the start of mixing, was concluded to be an important consideration.

It was suggested in the Lewis Aeropropulsion Conference[7] and later by Povinelli et al.[8] that convective effects arising from geometrically induced secondary flows play a more dominant role in the mixing process than previously anticipated. These effects arise from secondary flows at entry, which are sustained and amplified in the mixer passage by transverse pressure gradients. These conclusions were based on the computations performed with the viscous marching procedure described in Part I of this paper.[9] Subsequently, measurements performed by Patterson[10] clearly indicated the presence of radial outflow in the core region and radial inflow in the fan region at the lobe exit plane. In addition, some azumuthal component of the secondary flow was measured. Flow angularity measurements obtained at the Lewis Research Center were used to construct a representative secondary flowfield that depended only upon the bulk radial inflow and outflow velocities. This flowfield was used by Anderson et al.[11] as an initial condition for the mixer analysis. Use of this flowfield representation greatly simplified the task of specifying the point-by-point description of the lobe-generated secondary flow and clearly established the role of secondary flows in mixer nozzles. The radial inflow-outflow description of the initial secondary flowfield in the analysis gave rise to a strong vortex pattern aligned with the interface between the fan and core streams. This vortex system was convected downstream through the mixer nozzle. Comparison of the computed and measured total temperatures at the nozzle exit showed very good agreement.[11] The analysis was used to deduce the controlling mechanisms occuring in mixer nozzles, i.e., geometrically induced secondary flows are the dominant mixing mechanism. Subsequently, the mixer analysis was applied to several different lobe geometries by Anderson and Povinelli.[12] It was concluded that other secondary flow mechanisms might be present at the mixer entry which could influence the flowfield development.

In the present paper, the role of these additional secondary flow mechanisms is further explored using the three-dimensional turbulent analysis described in Part I.

Experimental Measurements

Apparatus

The test apparatus consisted of two basic parts: a fixed upstream model section and a rotating shroud. The upstream section simulated the flow path through a typical high by-pass turbofan engine. A cross section of the model is shown in Fig. 1. Heated air was supplied to the core passage and flowed through the lobe section. Unheated air was supplied to the fan

Received Dec. 21, 1981; revision received May 12, 1983.

*Head, Turbine Aerodynamics Section. Associate Fellow AIAA.
†Head, Aerodynamics Analysis Section. Member AIAA.

passage and measurements were taken with three different mixer configurations. The longitudinal contours of the three mixers are shown in Fig. 2. Each mixer had 12 lobes. Configurations A, B, and C have a penetration (lobe tip radius/shroud radius) of 0.822, 0.776, and 0.721 and a circumferential spacing ratio (core included angle/fan included angle) of 0.5, 1.0, and 1.36, respectively. The ratio of the shroud length to the inside shroud diameter (at the lobe exit plane) was 0.71.

Total pressure and temperature measurements were made upstream in both the fan and core flows. Instrumentation rakes were also mounted in the rotating shroud for probing the mixer flowfield (see Fig. 1). Total temperature rakes were located at five axial stations in the mixing region. The temperature data were obtained over a 54-deg segment in 3-deg increments at 14 radial positions. Flow angularity measurements using a fixed probe technique[13] were made at the two axial locations shown in Fig. 1.

The fan and core streams were operated with a total pressure ratio of 1 and a total temperature ratio, T_T/T_C, (fan/core) of 0.74 or 0.4. The Mach number of the fan and core streams at the mixing plane (lobe exit) was 0.45 and the bypass ratio was about 4. The Reynolds number based on shroud radius was 1.1×10^6.

Flow Angularity Measurements

The three velocity components near the exit plane of the lobes were measured using the flow angularity probes described in the Apparatus section. The flow angularity data were obtained in order to provide information about the mixer inflow conditions. The data were measured in a plane parallel to the exit plane of the lobes (see Fig. 1). Data were obtained at six radial locations and four circumferential positions within the measurement domain shown in Fig. 3 for the 12B and 12C lobe geometries. The vectors shown in Fig. 3 are the resultant of the measured radial and azimuthal velocities in a plane transverse to the mean flow. The maximum vector length in Fig. 3 corresponds to a velocity of 25% of the axial flow. Strong radial flows are evident with outflow in the core and inflow in the fan regions. It appears that a vortex-type flow is present at the fan-core interfacial regions. The flow angularity data were augmented using a four-point linear interpolation scheme. This interpolation of data was carried out in order to obtain a better graphical respresentation of the secondary flow structures at the lobe exit plane.

Computational Procedure

Analytical Method

The computer code used in this study of forced mixer nozzle aerodynamics is described in detail in Refs. 14-17. In this section, details arising from the application of the foregoing analysis to the turbofan mixer configuration described earlier are given. The cross section of this mixer geometry is presented in Fig. 4. The area immediately downstream of the nozzle plug tip is faired in with an assumed streamline to model the separated flow region expected in this mixer nozzle. Since the flow area excluded from consideration is small, this treatment is not believed to introduce significant error. The curvilinear coordinate system shown in Fig. 4 was constructed to fit the flow passage boundaries and has 21 streamwise nodal points, 40 radial nodes, and 11 azimuthal nodes. In planes of constant azimuth, orthogonal streamlines and velocity potential lines were constructed from a two-dimensional plane incompressible analysis.[18] This x-y coordinate system was then rotated about the mixer axis to form the axisymmetric coordinate system. Five reference stations are identified in Fig. 4, these correspond to the five experimental survey stations mentioned in the previous section. These are labeled 1, 8, 13, 17, and 21 and correspond to the computation nodal point nearest to the probing

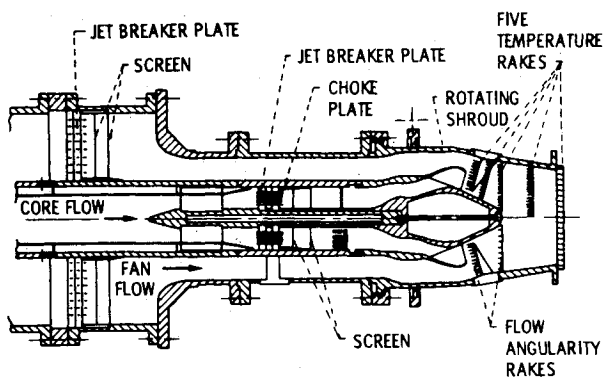

Fig. 1 Mixer nozzle cross section.

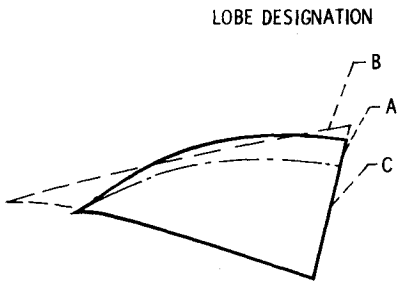

Fig. 2 Lobe geometry, longitudinal contours, 12 lobes.

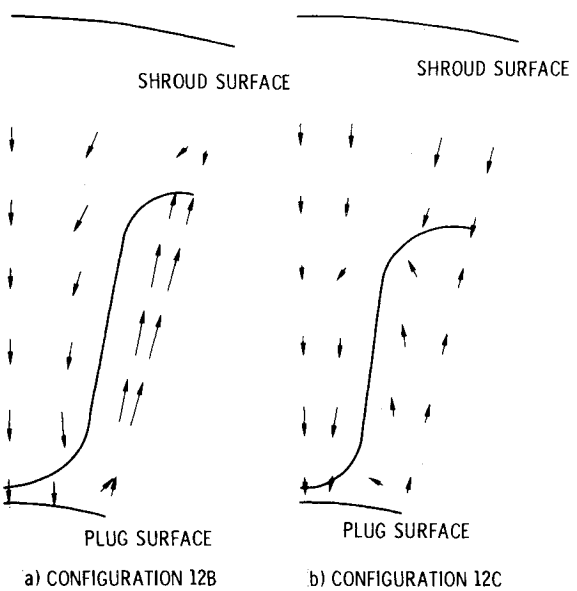

Fig. 3 Measured secondary velocity vectors, lobe exit station.

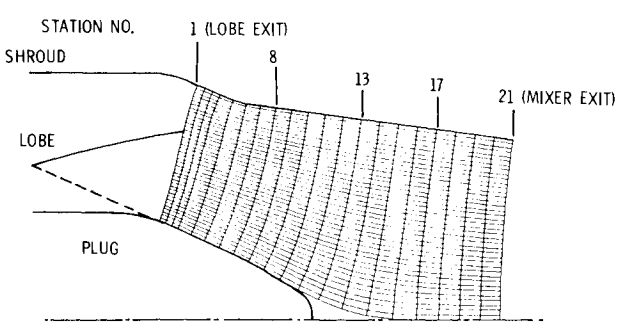

Fig. 4 Mixer nozzle computational mesh.

stations. Station 1 corresponds to the lobe exit station while station 21 is the mixer exit station.

Although the mixer geometry is periodic, the flow is three-dimensional due to the azimuthal variation of the hot and cold streams. However, due to observed symmetry, only a ½-lobe pie-shaped segment of the transverse coordinate surface was considered. The shape of this segment and the extent of typical hot and cold streams at the lobe exit station are shown in Fig. 5, as is a comparison between the computational and experimental lobe shape.

Secondary Flow Generation

Streamwise vorticity present at the entrance to the mixer passage is convected and diffused within the mixer passage and may be augmented or decreased by transverse pressure and density gradients and by deflection of the mean flow. Three mechanisms are postulated to be responsible for the generation of secondary flow within the lobes themselves. The most important one is due to the basic turning of the fan and core streams in opposite radial directions, as shown in Fig. 6. The secondary flow generation, termed "turning" or "flap vorticity," is basically an inviscid phenomenon and results in outward radial core flow adjacent to inward radial fan flow as shown in Fig. 6b. It is believed that this mechanism is properly represented in the starting conditions via the experimental flow angularity data obtained for each lobe geometry. The second mechanism responsible for secondary flow is "horseshoe" vorticity and is due to the interaction of upstream duct boundary layers with the lobe, which respresent flow obstructions, as shown conceptually in Fig. 7. The vorticity within the boundary layers encounters the lobes and vortex filaments wrap around the lobe in a horseshoe-like pattern. A set of vortices is subsequently set up in the fan flow and a set in the core flow. However, inspection of the experimental radial and tangential velocities at the lobe exit plane in the present experiments did not indicate that any significant effects were caused by this second mechanism. In addition, the low penetration lobes would tend to minimize the formation of strong horseshoe vortices. The third mechanism postulated is "passage" vorticity, which occurs as the core flow approaches the lobe exit and encounters the narrow gap between the centerbody and the bottom of the fan trough. As shown in Fig. 8, the vortex forms as flow washes up around the side of the fan troughs. The mechanism is similar to that occurring when flow approaches a slender cylindrical body at angle of attack. Tuft photographs taken of the inside surface of the lobes revealed a strong upward radial velocity component near the bottom of the lobe. Subsequent turning of the flow in the downstream direction occurs at a slightly larger radial position, as indicated by the tufts in Ref. 12. The behavior of the tufts strongly suggests the presence of a passage vortex. It was decided, therefore, to include a model for the passage vortex in the starting conditions for the computer code. In the absence of any measurements, a passage vortex strength based on a nominal percentage of the radial outflow velocity was assumed for an initial computation and developed into a consistent distribution over the inlet plane using the starting procedure defined in Part I. Subsequent estimates of the vortex strength were made and values of less than 10% of the radial outflow were sufficient to yield good agreement with experimental data in the final computations presented here. The presence of the passage vortex does not alter the secondary flow away from the plug

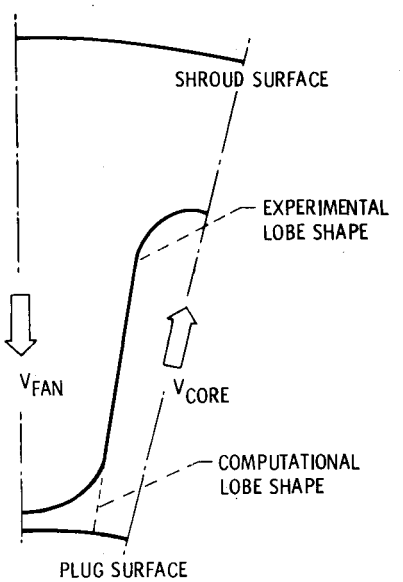

Fig. 5 Transverse computational segment.

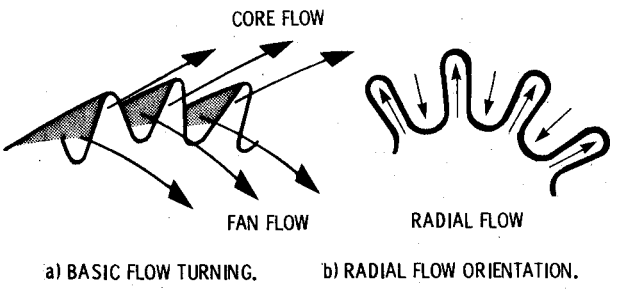

Fig. 6 Secondary flow generation, turning (flap) vorticity.

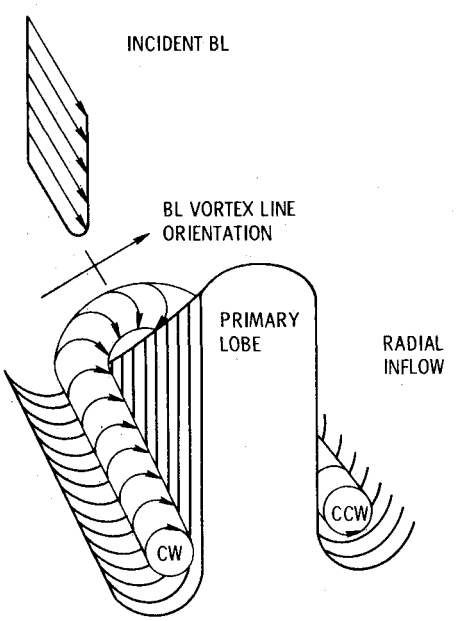

Fig. 7 Schematic representation of secondary stream horseshoe vortex formation (from Ref. 10, Fig. 30).

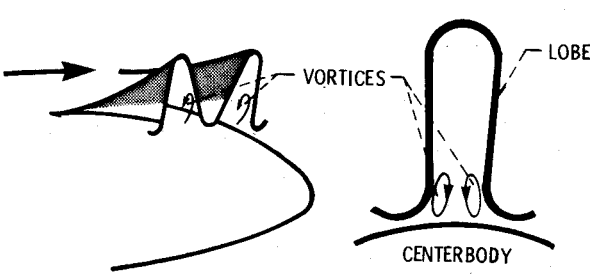

Fig. 8 Secondary flow generation, passage vortex.

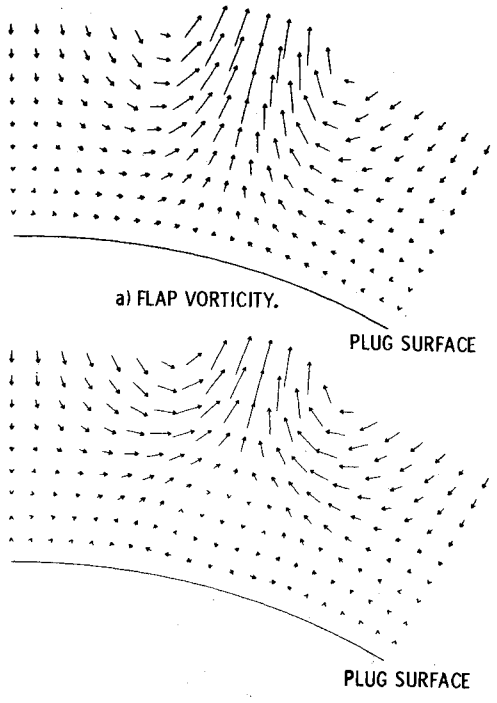

Fig. 9 Initial secondary flow field, lobe exit plane. 12B mixer, $T_C/T_F = 0.74$.

surface to any great extent, as seen in Fig. 9. It should be noted that the computational lobe shape, shown in Fig. 5, does not include a hot core layer between the centerbody and the bottom of the fan trough. Additional grid resolution in the code is required before the effect of this layer on the computations can be assessed.

Parametric Representation of the Inlet Flowfield

The secondary flow (flow transverse to the streamwise direction) is highly complex due to passage through the curved lobe section and currently precludes complete numerical simulation in the starting conditions. However, the large radial velocities of the starting secondary flow can be measured experimentally and simulated adequately. In this way, one simulates the large-scale secondary flow structure entering the mixer section by a parametric representation, based on a bulk radial velocity.

The representation of the large-scale flow transverse to the streamwise direction can be conceived as being composed of basically radial outflow in the core passage and radial inflow in the fan passage (Fig. 5). The mean radial outflow and inflow are distributed over the inlet plane as described in Part I. The experimental data for the mixer nozzle 12B configuration under study yielded radial velocities in the core and fan lobe passages of 25 and 20%, respectively, of the streamwise velocity. For the 12A and 12C geometries, the core flow was 14% and the fan flow was 8%. The streamwise velocity at each mesh point in the two respective streams was assigned its nondimensional reference value, which was then corrected to account for normal pressure gradients at the

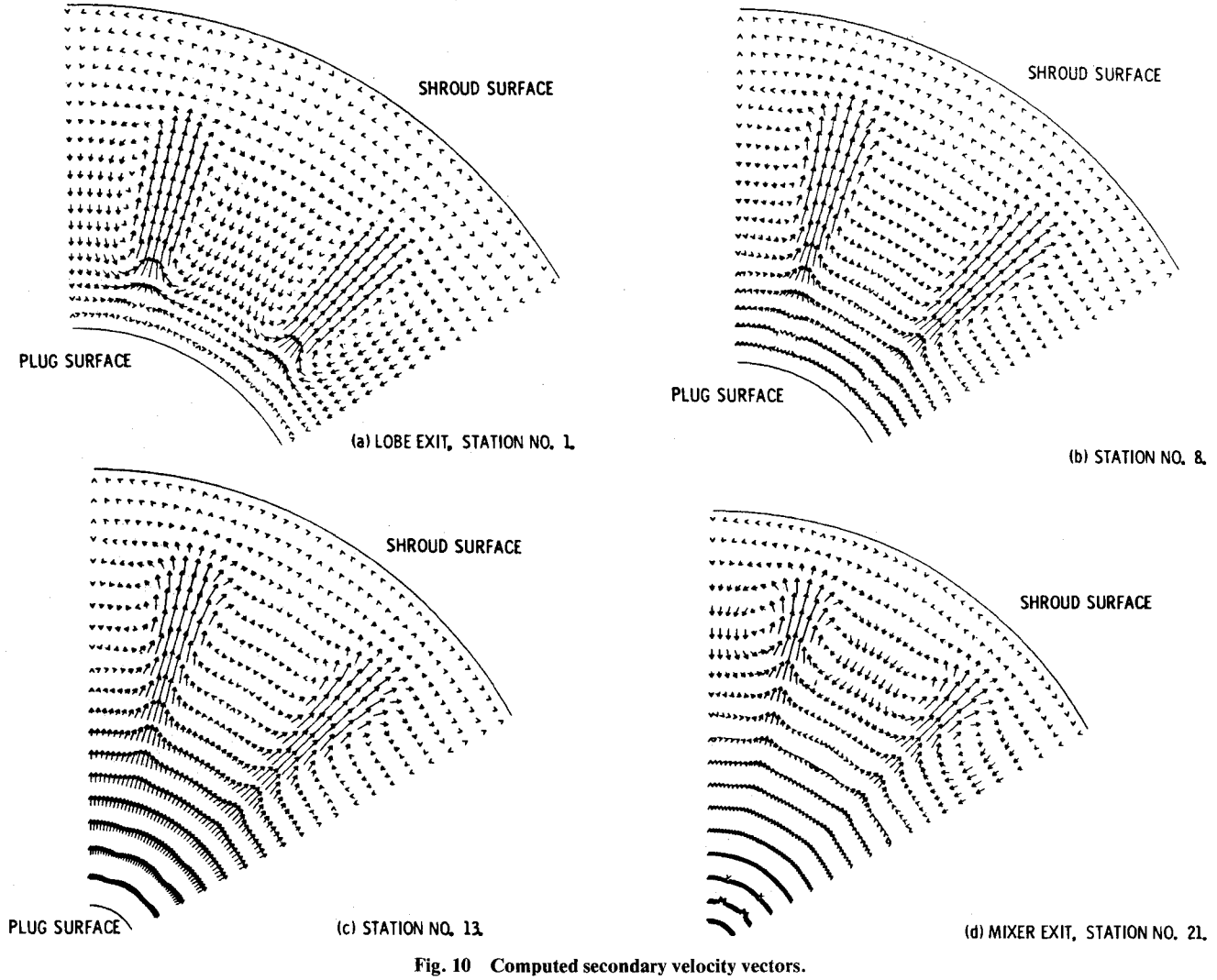

Fig. 10 Computed secondary velocity vectors.

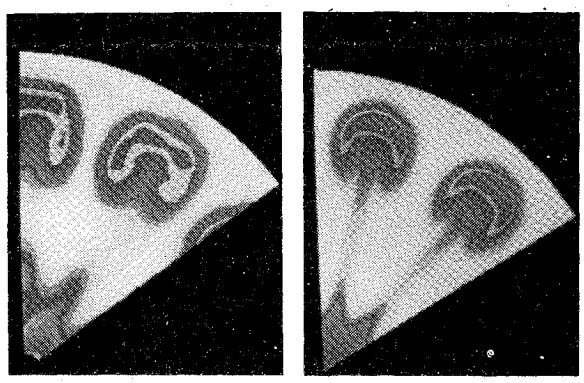

a) Experiment. b) Analysis.

Fig. 11 Comparison of total temperature contours at mixer exit plane.

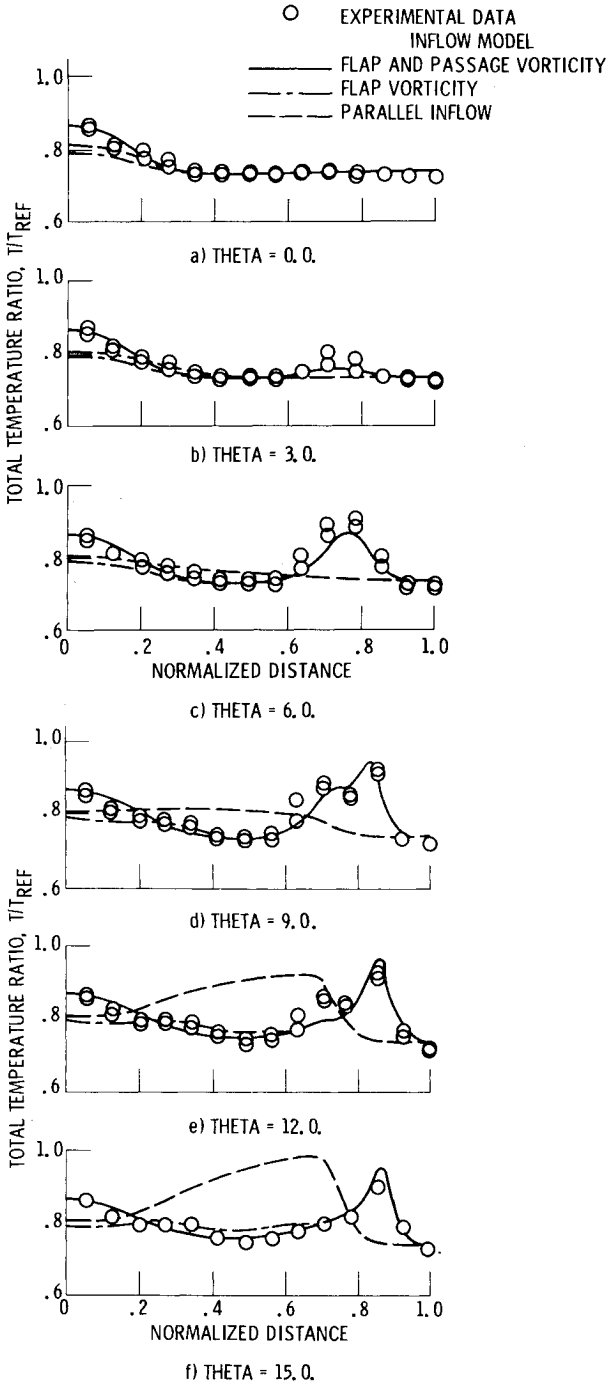

Fig. 12 Comparison of computed temperature profiles with experimental data. 12B mixer, $T_F/T_C = 0.74$, station 21.

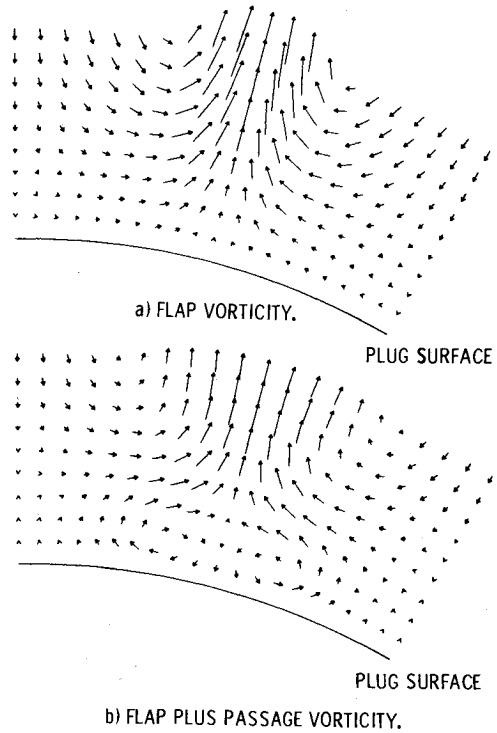

Fig. 13 Initial secondary flowfield, lobe exit plane. 12C mixer, $T_F/T_C = 0.74$.

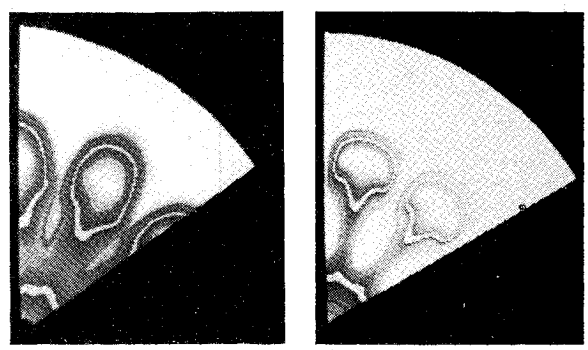

a) Experiment. b) Analysis.

Fig. 14 Comparison of total temperature contours at mixer exit plane.

initial plane as determined from the axisymmetric potential flow[1] To account for boundary layers on the lobe, plug, and shroud surface, the streamwise velocity profiles were further scaled in accordance with an assumed turbulent boundary-layer profile and distance from the lobe surface. Nondimensional boundary layers whose thickness is 5% of the shroud radius were used on all surfaces. The temperature field was constructed in the core and fan streams by assuming total temperature ratios $T_F/T_C = 0.74$ and 0.4, which correspond to the experimental temperature ratios. In addition, an entrance Mach number for each stream of 0.45 was assumed.

The turbulence quantities were initialized through specification of a length scale and freestream turbulence intensities. These turbulence quantities are assumed to be constant across the lobe shear layer but to vary with distance from the hub or shroud. For the calculations presented in this paper, the initial length scale was set at 0.006 of the outer shroud radius and turbulent intensity of both the core and fan streams was set at 4%. Previous results have shown that the nozzle exit temperature surveys were relatively insensitive to a turbulence level change from 4 to 12% (Fig. 20, Ref. 12). In addition, we have shown that both a two-equation and a wake turbulence model produced nearly identical results (i.e., Figs.

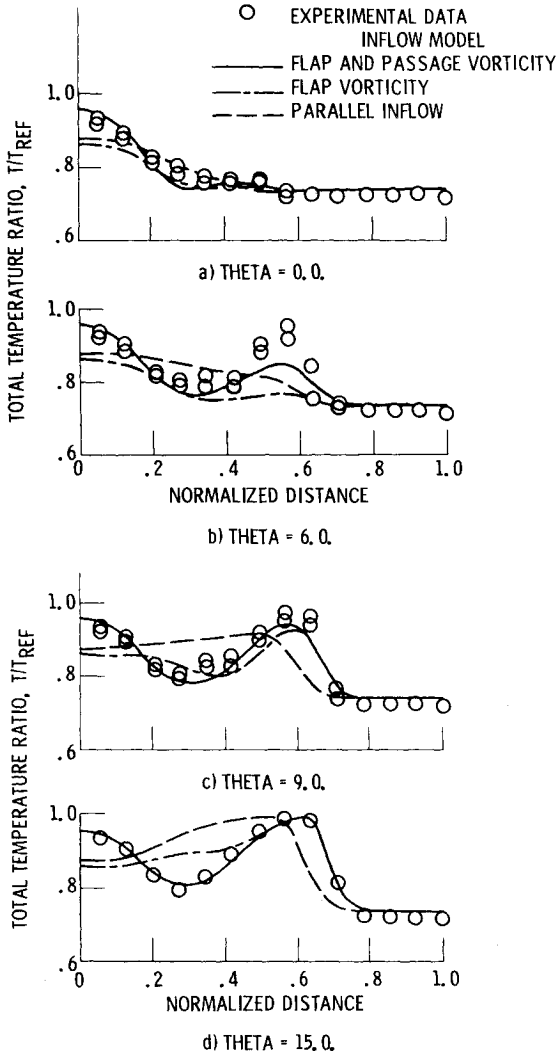

Fig. 15 Comparison of computed temperature profiles with experimental data. 12C mixer, $T_F/T_C = 0.74$, station 21.

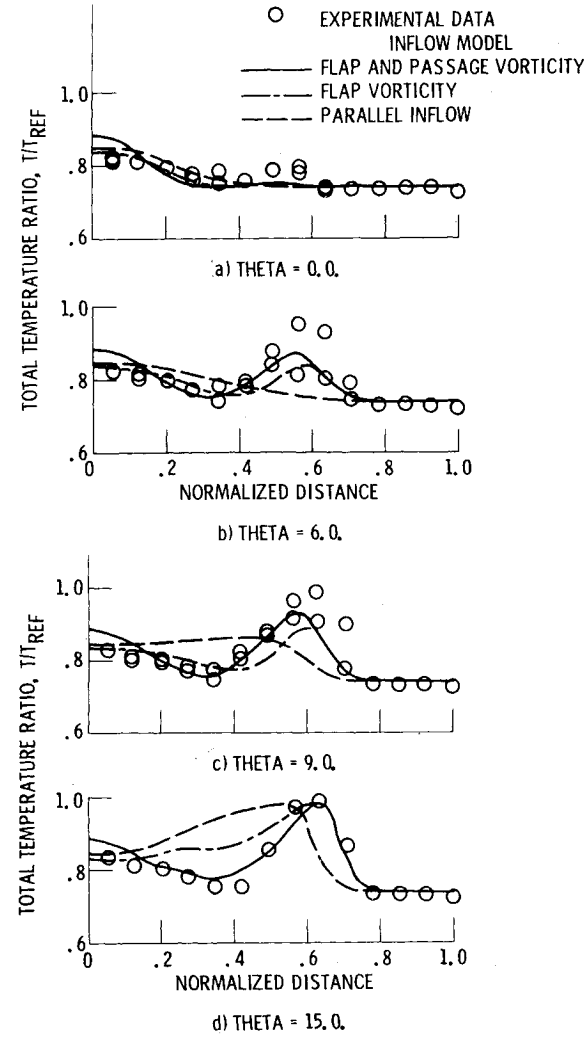

Fig. 16 Comparison of computed and experimental temperature profiles. 12A mixer, $T_F/T_C = 0.74$.

16 and 17 in Ref. 11). In this paper, therefore, only the wake turbulence results are shown.

Computational Results

Influence of Secondary Flowfield

Lobe B Mixer

The starting velocity vector field constructed according to the procedure described in the previous section is shown in Fig. 9 for the 12B mixer. Construction of the secondary velocity vector field was based on average radial velocities of 25 and 20% of the streamwise core and fan velocities, corresponding to the experimental data. Although the computational segment included only one half the lobe segment and one half the core passage, the computational results in Fig. 9 were reflected to represent one lobe and two fan regions. The secondary velocities presented are normal to the streamwise mesh coordinate and are shown only in the region near the plug (centerbody) surface. Figure 9a shows the flowfield modeling with flap vorticity only. Figure 9b shows the starting flowfield in which a set of passage vortices have been incorporated in the core flowfield along with the flap vorticity. These passage vortices are in the region between the plug surface and lower part of the lobe wall as described previously and shown in Fig. 8. The complete secondary flowfield at the starting plane, which is the lobe exit plane (see Fig. 4) is shown in Fig. 10a. The computational results were reflected to include two lobe and three fan regions as shown.

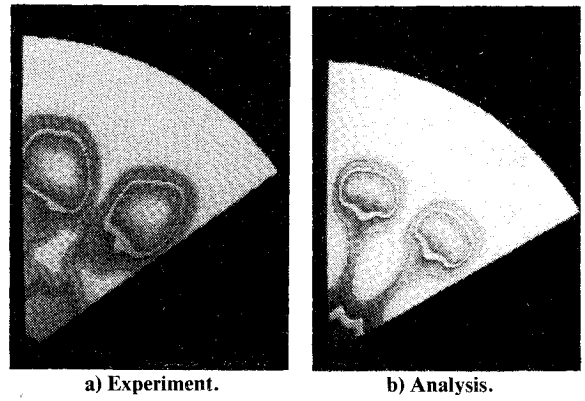

a) Experiment. b) Analysis.

Fig. 17 Comparison of total temperature contours at mixer exit plane.

A strong vortex pattern can be observed which is aligned with the interface region between the fan and core streams, as well as the small passage vortices near the plug surface. At station 8 (Fig. 10), which is located halfway along the plug, the vortex pattern begins to condense into a more circular pattern and moves radially outward. As indicated by the disappearance of radial inward flow near the plug surface the passage vortices disappear by station 13. The main vortex patten continues its outward movement (Figs. 10c-e). At the mixer exit plane (station 21) the vortex is still relatively strong.

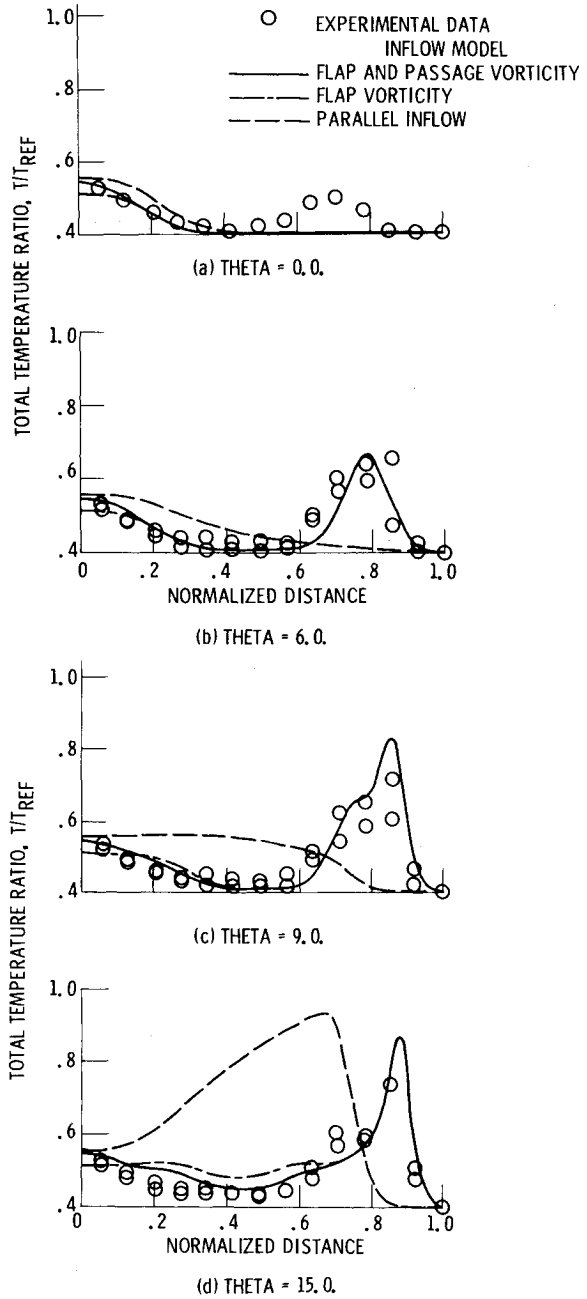

Fig. 18 Comparison of computed and experimental temperature profiles. 12B mixer, $T_F/T_C = 0.40$.

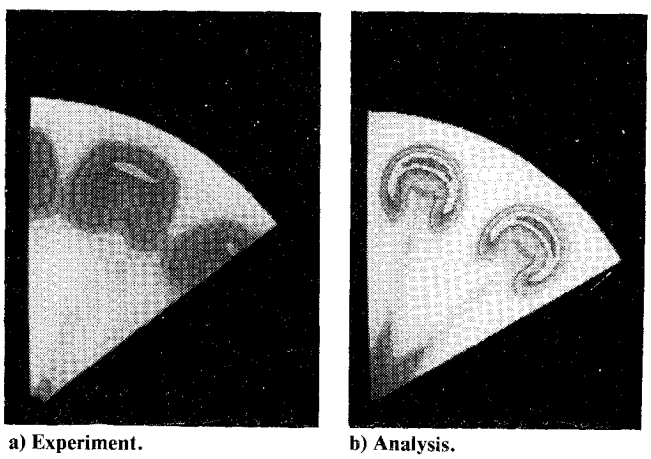

a) Experiment. b) Analysis.

Fig. 19 Comparison of total temperature contours at mixer exit plane.

A comparison between the measured and computed total temperature contours at the mixer exit plane (station 21) is presented in Fig. 11. The development of the horseshoe-shaped total temperature contour is clearly evident. This temperature signature is strongly influenced by the secondary flowfield as it develops downstream of the presecribed inflow conditions. Development of the colored image processing technique used is described in detail in Ref. 19.

A comparison between the measured and computed total temperature distributions at the mixer nozzle exit are presented in Fig. 12 for three rake positions. The centerline of the fan flow is at an angular value (θ) of 0 and the core flow centerline is at $\theta = 15$ deg. Computations were made assuming three different starting flowfield models: 1) parallel inflow conditions (no radial flow), 2) inflow with flap vorticity, and 3) inflow with both flap and passage vorticity. A comparison between the calculations using the flap and passage vorticity inflow pattern and the measured data show excellent agreement. The use of only flap vorticity yielded good agreement except over the first 20% of the radius. The strong influence of the secondary flow structure is evident by comparing the solid (secondary flowfields) with the dashed lines (parallel inflow). It is apparent that the characteristic horseshoe-shaped temperature signature resulted from the developing secondary flow structure initially established by the core and fan streams.

Lobe C Mixer

The corresponding data and computations for the 12C mixer are presented in Figs. 13-15. The starting velocity vector field is shown in Fig. 13 and is based on an average radial velocity of 13. 7 and 8% of the streamwise core and fan velocities, as determined from the experimental measurements. Figure 13a shows the flap vorticity model flowfield. Figure 13b shows the starting flowfield wherein the passage vorticity is also included. The qualitative features of the secondary flow pattern are similar to those shown previously for the 12B mixer. However, the magnitude of the radial flows is smaller and results in less radial displacement of the main vortices. Figure 14 shows both experimental and computed temperature contours at the nozzle exit plane, and these are in excellent agreement.

A comparison of the measured and computed total temperature distributions at the mixer nozzle exit is shown in Fig. 15 for two angular locations. In this comparison it is seen that the inflow condition with flap vorticity as well as the parallel inflow condition yield poor agreement with the experimental data, whereas the inflow condition with both flap and passage vorticity leads to excellent agreement. It is noted that the 12C mixer yields a radial temperature distribution distinctly different from that shown for the 12B in Fig. 12.

Lobe A Mixer

Radial temperature distributions at the mixer exit plane for the 12A mixer are shown in Fig. 16. As with the previous two geometries, the inflow condition with both flap and passage vorticity yields the best agreement with the data. The analysis appears to slightly underpredict temperature mixing over the inner 10% of the radius and to overpredict this mixing near the 60% point. However, it is noted that the two experimental data sets have significant scatter at the 60% radial position. Figure 17 shows the total temperature signatures from the experimental data and from the computations, and these are in good agreement.

Influence of Hot Core Temperature

The results presented in the previous section were based on warm flow testing where the ratio of fan-to-core stream total temperature was 0.740. In this section, the results from a fully simulated or hot flow condition with a temperature ratio of 0.40 was presented.

Computations were made using the three inflow models for the 12B mixer having a high temperature primary stream. The ratio of core-to-fan total temperature of 0.40 matches the experimental values used in the test program. The secondary velocity field was constructed using the same average radial velocities as in the previous calculations (Fig. 12). The primary velocity in the high-temperature stream was increased to obtain matched Mach numbers and total pressures in the two streams at the lobe exit plane. A comparison of the computed results with the experimental data is shown in Fig. 18. The comparison is at the mixer exit plane, that is, at station 21, and includes four angular locations from the centerline of the fan flow, $\theta = 0$, to the centerline of the curve flow, $\theta = 15$. As in the previous comparisons, the inflow condition having both flap and passage vorticity yields the best agreement. It is noted that the experimental data at the fan centerbody (Fig. 18a) show a small temperature rise at a normalized radius of 0.7, which was not present in the warm flow testing (see Fig. 12a). This rise indicates spreading of the primary stream into the center of the fan stream. The computer code apparently underpredicted the secondary flows and/or the temperature mixing in this region. Figure 19 presents the experimental and computed temperature contour information.

Concluding Remarks

The finite difference procedure presented in Part I of this paper has been used to compute the aerodynamic flow of three different experimental lobe geometries. For each geometry, experimental information was obtained at the lobe exit plane in order to provide initial conditions for the three-dimensional turbulent computations. The validity of the computer code was demonstrated by comparison of the nozzle exit temperature data with the computed three-dimensional temperature distributions.

The principal result from this study is that the complex flow structure found to exist in turbofan forced mixers is dominated by geometrically induced secondary flow rather than being turbulence controlled. The postulated mechanisms responsible for the generation of secondary flows at the lobe exit are: 1) the inviscid turning of the fan and turbine streams (flap vorticity), 2) turning due to turbine flow washing around the fan troughs in the vicinity of the centerbody (passage vorticity), and 3) horseshoe vorticity generated by the interaction of the turbine and fan flow boundary layers with the leading edges of the lobes.

Given a suitable representation of the initial conditions of the lobe exit plane, the capability of the computer code to predict the complex three-dimensional temperature contours within the mixing duct has been demonstrated. Even though this mixer code does not eliminate the current need for experimental investigations to define secondary flow conditions as input, this code can predict the parametric effect of different inflow conditions. When coupled to a future code (which accurately defines the flow conditions of both hot and cold streams as they approach the mixer nozzle exit plane for a specific mixer nozzle geometry), this code will provide the designer with an excellent method to evaluate the effectiveness of turbofan engine exhaust mixers without the costly expense of model testing.

References

[1] Frost, T. H., "Practical Bypass Mixing Systems for Fan Jet Aero Engines," *The Aeronautical Quarterly*, May 1966, pp. 141-160.

[2] Hartmann, A., "Studies of Mixing in Ducted Fanjet Engines," NASA Rept. TT F-12, 562, Nov. 1969.

[3] Schumpert, P. K., "An Experimental Model Investigation of Turbofan Engine Internal Exhaust Gas Mixer Configurations," AIAA Paper 80-0228, Jan. 1980.

[4] Koslowski, H. and Kraft, G., "Experimental Evaluation of Exhaust Mixers for an Energy Efficient Engine," AIAA Paper 80-1088, June 1980.

[5] Kuchar, A. P. and Chamberline, R., "Scale Model Performance Test Investigation of Exhaust System Mixers for an Energy Efficient Engine (E) Propulsion System," AIAA Paper 80-0229, Jan. 1980.

[6] Birch, S. F., Paynter, G. C., Spalding, D. B., and Tatchell, D. G., "Numerical Modeling of Three-Dimensional Flows in Turbofan Engine Exhaust Nozzles," *Journal of Aircraft*, Vol. 15, Aug. 1978, pp. 489-496.

[7] Bowditch, D. N., McNally, W. D., Anderson, B. H., Adamczyk, J. J., and Sockol, P. M., "Computational Fluid Mechanics of Internal Flow," Aeropropulsin 1979, NASA CP-2092, 1979, pp. 187-230.

[8] Povinelli, L. A., Anderson, B. H., and Gerstenmaier, W., "Computation of Three-Dimensional Flow in Turbofan Mixers and Comparison with Experimental Data," AIAA Paper 80-0227, Jan. 1980, NASA TM 81410.

[9] Kreskovsky, J. D., Briley, W. R., and McDonald, H., "Investigation of Mixing in a Turbofan Exhaust Duct, Part I: Analysis and Solution Procedure," *AIAA Journal*, Vol. 22, March 1984, pp. 374-382.

[10] Patterson, R. W., "Turbofan Forced Mixer-Nozzle Internal Flow Field, Vol.—A Benchmark Experimental Study," NASA CR, 1981.

[11] Anderson, B. H., Povinelli, L. A., and Gerstenmaier, W. G., "Influence of Pressure Driven Secondary Flows on the Behavior of Turbofan Forced Mixers," AIAA Paper 80-1198, June 1980; also, NASA TM-81541.

[12] Anderson, B. H. and Povinelli, L. A., "Factors Which Influence the Behavior of Turbofan Forced Mixer Nozzles," AIAA Paper 81-0274, Jan. 1981, NASA TM-81668.

[13] Dudzinski, T. J. and Krause, L. N., "Flow-Direction Measurement with Fixed-Position Probes," NASA TMX.

[14] Kreskovsky, J. P., Briley, W. R., and McDonald, H., "Turbofan Forced Mixer Nozzle Internal Flow Field, Vol. 3—A Computer Code for 3-D Mixing in Axisymmetric Nozzles," NASA CR, 1981.

[15] Briley, W. R., and McDonald, H., "Analysis and Computation of Viscous Subsonic Primary and Secondary Flows," *Proceedings, AIAA Computational Fluid Dynamics Conference*, New York, 1979, pp. 74-88.

[16] Kreskovsky, J. P., Briley, W. R., and McDonald, H., "Development of a Method for Computing Three-Dimensional Subsonic Turbulent Flows in Turbofan Lobe Mixers," Scientific Research Associates, Inc., Glastonburn, Conn., R79-300006-F, Nov. 1979.

[17] Kreskovsky, J. P., Briley, W. R., and McDonald, H., "Prediction of Laminar and Turbulent Primary and Secondary Flows in Strongly Curved Ducts," NASA CR-3388, Feb. 1981.

[18] Anderson, O. L., "Finite-Difference Solution for Turbulent Swirling Compressible Flow in Axisymmetric Ducts With Struts," NASA CR-2365, 1974.

[19] Anderson, B. H., Giamati, C. C., and Putt, C. W., "Application of Computer Generator Color Graphic Techniques to the Processing and Display of Three Dimensional Fluid Dynamic Data," ASME Annual Meeting, Washington, D.C., Nov. 1981.